This is the peer-reviewed, final accepted version for American Mineralogist, published by the Mineralogical Society of America.
The published version is subject to change. Cite as Authors (Year) Title. American Mineralogist, in press.
DOI: https://doi.org/10.2138/am-2021-7597. http://www.minsocam.org/

Revision 1

Non-linear Effects of Hydration on High-Pressure Sound Velocities of Rhyolitic Glasses

Jesse T. Gu[1], Suyu Fu[1], James E. Gardner[1], Shigeru Yamashita[2], Takuo Okuchi[2], Jung-Fu Lin[1]

[1]Department of Geological Sciences, Jackson School of Geosciences, The University of Texas at Austin, Austin, TX 78712, USA

[2]Institute for Planetary Materials, Okayama University, Misasa, Tottori 682-0193, Japan

Abstract

Acoustic compressional and shear wave velocities (V_P, V_S) of anhydrous (AHRG) and hydrous rhyolitic glasses containing 3.28 wt% (HRG-3) and 5.90 wt% (HRG-6) total water concentration (H_2O_t) have been measured using Brillouin Light Scattering (BLS) spectroscopy up to 3 GPa in a diamond anvil cell at ambient temperature. In addition, Fourier-transform infrared (FTIR) spectroscopy was used to measure the speciation of H_2O in the glasses up to 3 GPa. At ambient pressure, HRG-3 contains 1.58 (6) wt% hydroxyl groups (OH^-) and 1.70 (7) wt% molecular water (H_2O_m) while HRG-6 contains 1.67 (10) wt% OH^- and 4.23 (17) wt% H_2O_m where the numbers in parentheses are ±1σ. With increasing pressure, very little H_2O_m, if any, converts to OH^- within uncertainties in hydrous rhyolitic glasses such that HRG-6 contains much more H_2O_m than HRG-3 at all experimental pressures. We observe a non-linear relationship between high-pressure sound velocities and H_2O_t, which is attributed to the distinct effects of each water species on acoustic velocities and elastic moduli of hydrous glasses. Near ambient pressure, depolymerization due to OH^- reduces V_S and G more than V_P and K_S. V_P and K_S

in both anhydrous and hydrous glasses decrease with increasing pressure up to ~1-2 GPa before increasing with pressure. Above ~1-2 GPa, V_P and K_S in both hydrous glasses converge with those in AHRG. In particular, V_P in HRG-6 crosses over and becomes higher than V_P in AHRG. HRG-6 displays lower V_S and G than HRG-3 near ambient pressure, but V_S and G in these glasses converge above ~2 GPa. Our results show that hydrous rhyolitic glasses with ~2-4 wt% H_2O_m can be as incompressible as their anhydrous counterpart above ~1.5 GPa. The non-linear effects of hydration on high-pressure acoustic velocities and elastic moduli of rhyolitic glasses observed here may provide some insight into the behavior of hydrous silicate melts in felsic magma chambers at depth.

Keywords: hydrous glass, sound velocity, elasticity, water, rhyolite

Introduction

Igneous activity at Earth's surface significantly affects society and also shapes the physical and chemical properties of the crust (Carn et al. 2009). The role of "water" in igneous processes is a topic of great interest due to the widespread occurrence of H_2O in Earth's crust and mantle (Mysen and Richet 2005). H_2O is present in magmas and quenched silicate glasses as both molecular water (H_2O_m) and hydroxyl groups (OH^-), where OH^- depolymerizes the silicate network (Stolper 1982a, 1982b). Even at low concentrations, incorporation of these H_2O species has been shown to significantly alter the physical properties of glasses and melts, such as acoustic velocities and elastic moduli (Malfait et al. 2011; Whittington et al. 2012), melting temperature (Kushiro et al. 1968; Grove et al. 2012), density (Richet and Polian 1998; Ochs and Lange 1999; Richet et al. 2000), viscosity (Hess and Dingwell 1996; Richet et al. 1996; Whittington et al. 2000; Hui and Zhang 2007), chemical diffusivities (Behrens and Zhang 2001), and electrical conductivity (Ni et al. 2011; Guo et al. 2016). These effects are manifested in

explosive volcanic eruptions, some of the largest of which involve felsic magmas. The intensity of volcanic eruptions is largely governed by the viscosity of constituent magmas and, correspondingly, the degree to which the magmas are polymerized or depolymerized due to the presence of water species. While H_2O incorporated in silicate melts as OH^- depolymerizes the silicate network and decreases the viscosity of respective melts, it still plays an important role in explosive eruptions (Shaw 1963). H_2O solubility decreases during magma ascent and results in the exsolution of species into molecular H_2O vapor, which expands rapidly at magmatic temperatures (Moore et al. 1995). This process, in combination with the inherently high viscosity of anhydrous felsic magmas, causes the explosiveness of felsic, H_2O-rich magmas (Shaw 1972).

Felsic eruptions can occur when differentiation of partially melted lower crustal materials produce melts with high silica contents (Borg and Clynne 1998). These melts have been reported to contain as much as ~6-8 wt% H_2O_t at ~200-400 MPa and ~400-600°C (Lowenstern 1994; Wallace et al. 1999; Wallace 2005). Some of the largest felsic eruptions are supervolcanic eruptions that formed the Long Valley and Yellowstone calderas (Bailey et al. 1976; Crosweller et al. 2012). Others felsic eruptions occur along subduction zones, like in the Andes, Japan, and the Cascades (Wallace 2005; Kimura et al. 2015; Brandmeier and Wörner 2016). Although seismic observations can give insight into pre-eruptive processes, the detection and estimation of crustal melt volumes and volatile contents under extreme pressure-temperature (P-T) conditions remains challenging (Flinders and Shen 2017; Flinders et al. 2018). Understanding the acoustic velocities in glasses of relevant compositions and the role of different species of H_2O on altering these velocities with depth can aid in constraining and interpreting melt fractions and volatile contents of magmatic bodies observed from seismic studies. Furthermore, uncovering physical

properties, such as density and incompressibility, of rhyolitic melts at depth is essential to our interpretation of eruptive processes, such as melt buoyancy and melt migration.

Two previous studies have focused on the effect of H_2O on the elastic properties of quenched haplogranitic and rhyolitic glasses at ambient pressure (Malfait et al. 2011; Whittington et al. 2012). Other experimental studies have explored the elastic properties of anhydrous silicate glasses of various compositions at high pressure (Meister et al. 1980; Suito et al. 1992; Zha et al. 1994; Sanchez-Valle and Bass 2010; Yokoyama et al. 2010; Liu and Lin 2014; Clark et al. 2016). These studies have shown that silicate glasses exhibit anomalous elastic properties with increasing pressure. In crystalline materials, acoustic velocities and elastic parameters normally increase approximately linearly with pressure. In silicate glasses, however, these properties decrease with pressure up to ~2-5 GPa, but then increase with pressure above a certain transition pressure. This minima in elastic properties has been attributed to the anomalous compression mechanisms in silicate glasses, whereby densification results from tightening of inter-tetrahedral bond angles and a distortion of the tetrahedral network rather than by decreasing bond lengths (Clark et al. 2014; Wang et al. 2014). The minima in velocities and compressibility correspond to pressures at which silicate glasses reach a packing limit. At higher pressures, densification occurs through shortening of bond lengths and increasing Al and Si coordination. The pressure dependence of the increasing coordination is dependent upon the composition and polymerization of the glass (Lee et al. 2004, 2011; Lee and Stebbins 2009). The presence of volatiles in interstitial voids can affect the velocity minima and the transition pressure of the glass (Clark et al. 2016). Therefore, the linear effects of water on acoustic velocities of hydrous glasses observed near ambient pressure in previous studies (Malfait et al. 2011; Whittington et al. 2012) may not hold at high pressure and need to be investigated.

This is the peer-reviewed, final accepted version for American Mineralogist, published by the Mineralogical Society of America.
The published version is subject to change. Cite as Authors (Year) Title. American Mineralogist, in press.
DOI: https://doi.org/10.2138/am-2021-7597. http://www.minsocam.org/

The polymerization of hydrous rhyolitic melts and glasses may also change if the proportion of OH^- to H_2O_m changes as a function of pressure and temperature. The relative proportion of H_2O_m and OH^- have been shown to change at high pressures above ~1.0 GPa and could alter the structure and elastic properties of hydrous glasses and melts at higher pressures (Ihinger et al. 1999; Hui et al. 2008; Malfait et al. 2012; Ardia et al. 2014; Helwig et al. 2016). With increasing temperature, the ratio of OH^- to H_2O_m will increase, and OH^- will dominate at magmatic temperatures (Stolper 1982a; Keppler and Bagdassarov 1993; Nowak and Behrens 1995; Shen and Keppler 1995). Because studying the properties of melts at high pressure and temperature conditions remains challenging, silicate glasses have commonly been used as analogues for silicate melts (Williams and Jeanloz 1998; Lee et al. 2008). Previous studies have shown that quenched glasses retain the local structure of their corresponding liquids (Seifert et al. 1981; Malfait et al. 2014), which has been commonly used as justification for the analogue approach.

Despite previous efforts, the effects of H_2O_m and OH^- on the acoustic velocities and elastic moduli of rhyolitic glasses at pressures above a few hundred megapascals have been poorly studied. At pressures relevant to felsic magma chambers, elastic properties depend not only on H_2O_t, but also on how the different species of H_2O interact with the structure of the glass. The linear hydration effect on acoustic velocities of rhyolitic glasses observed previously at ambient pressure (Malfait et al. 2011; Whittington et al. 2012) could become non-linear at high pressures. In order to better understand the behavior of felsic magmas at depth, it is thus essential to constrain water speciation in hydrous glasses and correlate these species with experimental acoustic velocities and elastic moduli at high pressures.

Here, we report acoustic velocities and elastic moduli in both anhydrous (AHRG) and hydrous rhyolitic glasses containing 3.28 wt% H_2O_t (HRG-3) and 5.90 wt% H_2O_t (HRG-6), measured using Brillouin Light Scattering (BLS) spectroscopy in a diamond anvil cell (DAC) up to 3 GPa. Complementary FTIR measurements were also conducted to examine H_2O speciation as a function of pressure. These observations are applied to correlate how the different species of H_2O contribute to the observed changes in velocities and equation of state parameters of hydrous rhyolitic glasses at high pressures. We observe non-linear effects of hydration on acoustic velocities and elastic moduli at high pressure, which are applied to decipher elastic behaviors of felsic magmas in the deep crust.

Experimental Methods

Rhyolitic glass samples were cored from a natural obsidian, which consisted of high-silica rhyolitic glass and less than 1 vol% microlites of Fe-Ti oxides (Gardner and Ketcham 2011). Two cores were placed in Au capsules, along with a pre-determined amount of deionized water to ensure H_2O-saturation at run conditions. The capsules were welded shut and then heated and weighed to ensure that no leaks existed. The samples were then run in externally heated pressure vessels at high P-T conditions for approximately 7 days in the Petrology Laboratory of the University of Texas at Austin (Table 1). A third core was placed inside a Pt capsule for the synthesis of anhydrous rhyolitic glass (AHRG), which was left open, and was placed inside an externally heated pressure vessel and run at 0.5 MPa and 1150°C in Ar gas to dehydrate the glass sample. All samples were quenched rapidly, and the two runs at elevated pressures were weighed to check for leaks. After quenching, sample compositions and homogeneity were evaluated by the JEOL JXA-8200 Electron Microprobe in the Department of Geological Sciences at The University of Texas at Austin (Table 2). At least 10 measurements of each glass sample were

made with an accelerating voltage of 10 kV, beam currents of 2-10 nA, and defocused beam sizes of 10-20 μm. Oxide compositions were averaged and normalized to 100% for comparison between different glass samples (Table 2). In total, three samples were synthesized and used for the study: one glass with 3.28 wt% H_2O_t (HRG-3) and one glass with 5.90 wt% H_2O_t (HRG-6), while the third core produced anhydrous glass with ~0.1 wt% H_2O_t (AHRG) (Table 1).

FTIR analyses of double-polished samples at ambient conditions were carried out on all glass samples in the Department of Geological Sciences at The University of Texas at Austin to determine H_2O_t using a Thermo Electron Nicolet 6700 spectrometer and Continuum IR microscope. Absorbances in the near-infrared region at ~4500 cm^{-1} and ~5200 cm^{-1} were used to calculate H_2O_t at ambient conditions following the procedures of Gardner and Ketcham (2011). At ambient pressure, AHRG contains ~0.1 wt% H_2O_t, HRG-3 contains 1.58 (6) wt% OH^- and 1.70 (7) wt% H_2O_m, and HRG-6 contains 1.67 (10) wt% OH^- and 4.23 (17) wt% H_2O_m. The water content in AHRG is negligible compared to the two hydrous glasses so it is used as the reference for the anhydrous rhyolitic glass.

Furthermore, densities at ambient pressure (ρ_0) for the glasses were determined from the partial molar volumes of oxide components and H_2O at 300 K following literature procedures (Richet et al. 2000; Lin and Liu 2006). Archimedes' method with toluene as the immersion liquid was used to confirm that the density of HRG-6 matched the calculated density within uncertainties. The other two glass samples, AHRG and HRG-3, were not checked with this method because of insufficient quantities of materials.

Two runs of micro-FTIR measurements at high pressure were carried out on all glass samples in DACs at the Institute for Planetary Materials, Okayama University in Misasa, Japan. Micro-FTIR measurements were taken using a Jasco FTIR-6200 Fourier-transform spectrometer

158 fitted with a Jasco IRT-7000 microscope with Cassegrain optics (Chertkova and Yamashita
159 2015). Transmitted light was received by a LN_2-cooled HgCdTe detector for both mid-infrared
160 (MIR) and near-infrared (NIR) measurements. Analytical procedures were similar to those
161 described in Chertkova and Yamashita (2015), except a CaF_2/Si beamsplitter was used for NIR
162 measurements while a KBr/Ge beamsplitter was used for MIR measurements. Glass sample
163 platelets were prepared by polishing both sides using 3M diamond films with 1 μm and 0.3 μm
164 grain sizes. Ambient pressure spectra in the NIR region were recorded to confirm H_2O_t in the
165 glasses and to compare with MIR spectra before high-pressure runs (Figure 1). H_2O speciation in
166 HRG-6 calculated using MIR and NIR spectra agreed well within uncertainties. In high-pressure
167 measurements, background spectra of the diamond anvils and the sample chamber were taken
168 prior to each measurement and were subsequently subtracted from the recorded spectra
169 (Chertkova and Yamashita 2015). In the first run (FTIR-Run 1), a 250 μm thick Re gasket with a
170 300 μm hole in the center was pre-indented to a thickness of ~100 μm and was sandwiched
171 between diamond anvils with diameters of 600 μm in a DAC. One piece of AHRG that was 23 ±
172 3 μm thick and one piece of HRG-6 that was 28 ± 3 μm thick were simultaneously loaded into
173 the DAC along with Ne and a ruby sphere as pressure medium and pressure calibrant,
174 respectively (Dewaele et al. 2008). The MIR region from 1400-4000 cm^{-1} was used in this run to
175 measure H_2O_t and H_2O_m in the glasses (Figure 1). OH^- contents were then calculated based on
176 the difference between H_2O_t and H_2O_m. In the second run (FTIR-Run 2), a DAC with a pair of
177 750 μm culets was equipped with a 500 μm thick Re gasket pre-indented to ~400 μm with a 650
178 μm hole in the center. A 333 ± 3 μm thick piece of HRG-3 was loaded into the DAC along with
179 Ne and a ruby sphere. The large thickness of the sample resulted in saturated absorption bands in

the MIR region, so bands in the NIR region from 4000-6000 cm^{-1} were used to measure H_2O speciation instead (Figure 1).

Three separate runs of BLS measurements were carried out on the glasses up to 3 GPa in DACs (Figure 2). Each DAC with a pair of 600 μm culets was equipped with a 250 μm thick Re gasket pre-indented to ~150 μm with a 300 μm hole in the center. Glass samples with diameters of ~100 μm were double-polished down to <70 μm thick using 3M diamond films with 1 μm and 0.3 μm grain sizes. The samples were then placed in a sample chamber with either Ne or 4:1 methanol:ethanol as the pressure medium (Figure 2). It has been proposed that the use of noble gases pressure media could alter the compressibilities and measured velocities in silicate glasses (Shen et al. 2011; Weigel et al. 2012; Clark et al. 2014; Coasne et al. 2014), so 4:1 methanol:ethanol was used as the pressure medium in a separate run to check for these effects. Both AHRG and HRG-6 were loaded simultaneously in the first (BLS-Run 1) and second (BLS-Run 2) runs with Ne and 4:1 methanol:ethanol, respectively. In the third run (BLS-Run 3), HRG-3 was loaded with Ne as the pressure medium. In all runs, a ruby sphere was used as the pressure calibrant (Dewaele et al. 2008).

BLS measurements were taken at the Mineral Physics Laboratory in the Department of Geological Sciences at The University of Texas at Austin. The Brillouin system is equipped with a 532 nm Coherent Verdi V2 laser and a JRS six-pass tandem Fabry-Perot interferometer (Lu et al. 2013; Yang et al. 2014; Fu et al. 2017). The focused beam size at the sample position was ~30 μm. Spectra were collected in a symmetric forward scattering geometry with an external angle of 48.1°. The system is calibrated monthly using standard distilled water and silica glass (Lu et al. 2013). Acoustic velocities were calculated from the measured frequency shift from:

This is the peer-reviewed, final accepted version for American Mineralogist, published by the Mineralogical Society of America.
The published version is subject to change. Cite as Authors (Year) Title. American Mineralogist, in press.
DOI: https://doi.org/10.2138/am-2021-7597. http://www.minsocam.org/

$$V_{P,S} = \frac{\Delta \upsilon_B \lambda_0}{2sin(\theta/2)}$$

where $V_{P,S}$ is the compressional (V_P) or shear (V_S) velocity, $\Delta\upsilon_B$ is the measured Brillouin shift, λ_0 is the laser wavelength in vacuum (approximately the same as in air) (532 nm), and θ is the external scattering angle (48.1°). Representative Brillouin spectra of rhyolitic glasses at high pressure are shown in Figure 2.

Data Analysis and Modeling

Measured acoustic velocities from BLS were used to derive other elastic parameters, including density (ρ), adiabatic bulk moduli (K_S), and shear moduli (G) (Sanchez-Valle and Bass 2010; Liu and Lin 2014). To derive these elastic moduli from velocity data, it is first necessary to determine the density of the glasses as a function of pressure. Assuming the glass samples behave elastically under compression, the density of the glasses at high pressures can be derived from:

$$\rho - \rho_0 = \int_{P_0}^{P} \frac{1}{(V_p^2 - \frac{4}{3}V_s^2)} dP$$

where ρ is the density of the glass at high pressure, ρ_0 is the density of the glass at ambient pressure (0.1 MPa), and P is the pressure (Sanchez-Valle and Bass 2010; Liu and Lin 2014; Sakamaki et al. 2014). Once acoustic velocities and densities at corresponding pressures were determined, the elastic moduli, were determined from:

$$K_S = \rho(V_p^2 - \frac{4}{3}V_s^2)$$

$$G = \rho V_s^2$$

This is the peer-reviewed, final accepted version for American Mineralogist, published by the Mineralogical Society of America.
The published version is subject to change. Cite as Authors (Year) Title. American Mineralogist, in press.
DOI: https://doi.org/10.2138/am-2021-7597. http://www.minsocam.org/

Fourth-order Eulerian finite-strain EoS (Birch 1978) were then fit to the derived elastic moduli. The fourth-order EoS was used to better capture the anomalous incompressibility and non-linear change in K_S and G in silicate glasses with increasing pressure (Clark et al. 2014; Liu and Lin 2014). Fitted elastic moduli are also used to simultaneously fit measured acoustic velocities as a function of pressure up to 3 GPa.

Measured FTIR spectra were analyzed to calculate H_2O speciation of the samples as a function of pressure via the Beer-Lambert law, which relates absorbance and thickness of a material to the concentration of the absorbing species within it (Newman et al. 1986; Ihinger et al. 1999; McIntosh et al. 2017), according to:

$$C_{H_2O_{t,m},OH} = \frac{M * A}{\rho * t * \varepsilon}$$

where $C_{H_2O_{t,m},OH}$ is the concentration of either H_2O_t, H_2O_m, or H_2O dissolved as OH^-, M is the molar mass of the species of interest, A is the absorbance, ρ is density of the glass, t is thickness of the glass, and ε is the molar absorption coefficient of the FTIR band of interest (Figure 3). ε in rhyolitic glasses has been studied extensively in both MIR and NIR regions (Newman et al. 1986; Zhang et al. 1997; Withers et al. 1999; McIntosh et al. 2017). Both MIR and NIR calibrations result in the same H_2O speciation, within uncertainties, in HRG-6 at ambient pressure. Therefore, both IR regions are suitable for calculation of H_2O speciation at high pressure. Density of glass samples as a function of pressure were determined from equation of state (EoS) fitting. Because glass is elastically isotropic, the thickness of a sample at high pressure is determined from:

$$t = t_0 \sqrt[3]{\frac{\rho_0}{\rho}}$$

where t_0 is the sample thickness in μm at ambient pressure that was measured using an optical microscope (Amin et al. 2012). The MIR region was used to determine the H_2O speciation HRG-6. The area under the peaks at ~1600 cm^{-1} and ~3500 cm^{-1} were determined after a linear baseline was subtracted from the raw spectra (Newman et al. 1986). The species-dependent method of determining H_2O_t from the band at ~3500 cm^{-1} was used along with molar absorption coefficients from Newman et al. (1986) and McIntosh et al. (2017). Because of the thickness of HRG-3, the bands in the MIR region were saturated. The ~4500 cm^{-1} and ~5200 cm^{-1} peaks in the NIR region were therefore used instead to determine H_2O speciation. However, the sample was bridged and crushed by the diamond anvils at ~1.5 GPa, so no spectra were recorded above this pressure. Using published values for the molar absorption coefficients, the speciation of H_2O_m and OH^- were determined from the area under the peaks at ~4500 cm^{-1} and ~5200 cm^{-1} after a flexicurve baseline was subtracted from the raw spectra (Figure 3) (Withers and Behrens 1999).

Results

Analysis of BLS and FTIR results show that the addition of H_2O into rhyolitic glasses decreases V_P and V_S in hydrous glasses at ambient pressure, consistent with previous studies (Figure 4) (Malfait et al. 2011; Whittington et al. 2012). Compared to AHRG at ambient pressure, V_P (V_S) in HRG-3 and HRG-6 are reduced by ~4.8% (~6.7%) and ~5.1% (~8.6%), respectively (Table 3). Our results are consistent with those of rhyolitic glasses in previous studies and show slightly larger reductions in velocities compared to haplogranitic glasses (Meister et al. 1980; Suito et al. 1992; Malfait et al. 2011; Whittington et al. 2012). In addition, reductions in velocities due to hydration are larger in V_S than those in V_P. The larger reductions in V_S can be attributed to depolymerization of the glass structure by OH^-, which reduces its shear-

resistance (Stolper 1982b, 1982a; Deschamps et al. 2011). V_P, on the other hand, is not affected as much because the bulk compressibility of the glass structure is not altered as much by H_2O_m in interstitial voids or by depolymerization due to OH^-.

The pressure dependence of H_2O speciation was determined from analysis of high-pressure FTIR spectra (Figure 3). Spectral features in high-pressure FTIR spectra are generally consistent with those observed at ambient pressure. Broadening of the band at ~3250 cm^{-1}, however, is interpreted to result from pressure-induced broadening of the absorption band. Similarly, pressure appears to shift the band at ~4500 cm^{-1} to lower wavenumbers. Despite these slight modifications, calculated H_2O_t remain constant within uncertainties at high pressure. With increasing pressure, very little, if any, H_2O_m in HRG-6 appears to be converted into OH^- (Figure 5). Conversion of water species is not resolvable due to the large uncertainties in our calculated species abundances. If present, this conversion mostly occurs below 1.5 GPa in HRG-6. In glasses with low H_2O_t (<4 wt%), the conversion from H_2O_m to OH^- has only been observed above 1 GPa in previous studies (Hui et al. 2008). In contrast, HRG-3 shows almost no change in speciation up to ~1.5 GPa (Figure 5). Even if HRG-3 undergoes changes in speciation above ~1.5 GPa, as reported in the literature, the quantity of change will not be large and the relative ratio of OH^- to H_2O_m will remain relatively constant. At all pressures, HRG-6 will contain more than a factor of two more H_2O_m than HRG-3, whereas their OH^- contents will remain similar. Therefore, differences in behavior between HRG-3 and HRG-6 can almost entirely be attributed to the excess H_2O_m in HRG-6. These samples allow us to investigate the effects of water species on velocities and elastic moduli of rhyolitic glasses at high pressure without having to consider changes in speciation.

This is the peer-reviewed, final accepted version for American Mineralogist, published by the Mineralogical Society of America.
The published version is subject to change. Cite as Authors (Year) Title. American Mineralogist, in press.
DOI: https://doi.org/10.2138/am-2021-7597. http://www.minsocam.org/

Measured V_P and V_S of the three glasses display non-linear and negative slopes with increasing pressure up to ~1-2 GPa (Figure 6). V_S in HRG-6 shows a minimum and increases above ~2 GPa whereas V_S in both AHRG and HRG-3 decrease throughout the whole experimental pressure range. On the contrary, there is a minimum in V_P below 3 GPa in all glass samples. The anomalous pressure dependence of velocities is consistent with previous studies on silicate glasses (Sanchez-Valle and Bass 2010; Clark et al. 2014; Liu and Lin 2014). The pressure at which acoustic velocities reach their minima in glasses is termed in the literature as the "transition" pressure and has been shown to occur at lower pressures due to the presence of volatiles (Weigel et al. 2012; Coasne et al. 2014; Liu and Lin 2014; Clark et al. 2016). In rhyolitic glasses, this transition pressure decreases in the hydrous glasses, such that the transition in V_P occurs at ~1-1.5 GPa in HRG-3 and HRG-6 whereas it occurs at ~2 GPa in AHRG. The lower transition pressure in hydrous glasses causes V_P and V_S in hydrous glasses to converge with those in AHRG (Figure 6c). In other words, velocity differences (ΔV_P and ΔV_S) between hydrous glasses and AHRG become less negative at high pressure. Eventually, V_P in HRG-6 crosses over and becomes higher than V_P in both HRG-3 and AHRG. Based on the modeled velocities, the crossover in V_P between AHRG and HRG-3 occurs above 3 GPa. V_S of HRG-6 converges with that of HRG-3 and eventually becomes indistinguishable from HRG-3 above ~2 GPa. Crossovers in V_S between hydrous glasses and their anhydrous counterpart appear to occur above 3 GPa. Despite differences in transition pressures between V_P and V_S and even though ΔV_S remains ~4% lower than ΔV_P, both ΔV_P and ΔV_S in hydrous glasses display remarkably similar trends at high pressure (Figure 6c). The convergence of ΔV_P and ΔV_S at different rates between all three samples produces non-linear effects of hydration at high pressure.

303 The derived densities of hydrous rhyolitic glasses at ambient pressure are consistent with
304 reported densities of haplogranitic and rhyolitic glasses (Figure 7) (Malfait et al. 2011;
305 Whittington et al. 2012). These observations show decreasing density with the addition of H_2O_t
306 where increasing H_2O_t by 1 wt% reduces density by ~0.5-0.6%. In contrast, the derived high-
307 pressure densities are higher than those observed in haplogranitic glasses quenched from high
308 pressures and measured at ambient pressure (Ardia et al. 2014). Despite these differences, we
309 observe similar trends in the density differences ($\Delta\rho$) between hydrous glasses and AHRG where
310 the difference in density due to hydration increases above ~1.5 GPa (Figure 7 inset). The
311 modeled elastic moduli of the glasses also show anomalous behavior at high pressure due to
312 hydration and correspond to the density trends above ~1.5 GPa (Figure 8). The addition of H_2O
313 decreases both K_S and G below ~1.5 GPa (Table 3). At these pressures, K_S is virtually
314 indistinguishable between HRG-3 and HRG-6, whereas the reduction in G due to hydration
315 between HRG-3 and HRG-6 is discernible. Above ~1-1.5 GPa, K_S in all three glasses converge
316 and become virtually indistinguishable from each other. This convergence causes K_S in hydrous
317 glasses to increase more rapidly than in AHRG and results in a slight increase in $\Delta\rho$ in hydrous
318 glasses (Figure 7 inset). In G, however, HRG-3 and HRG-6 begin to converge with AHRG above
319 ~2 GPa but remain distinctly lower. It is possible that convergence of G between hydrous glasses
320 and their anhydrous counterpart occur at higher pressures. The pressure-dependence of K_S is
321 more similar to that of V_P whereas the pressure-dependence of G is more comparable to that of
322 V_S.

323 Previous studies have reported that the use of noble gases (He or Ne) as pressure media
324 can significantly alter the observed elastic properties in silicate glasses (Shen et al. 2011; Weigel
325 et al. 2012; Clark et al. 2014; Coasne et al. 2014). These effects have been attributed to the

adsorption of noble gas molecules into interstitial sites in silicate glasses, which stiffens the glass network, making it more incompressible. The difference between our results using the two pressure transmitting media is, however, much smaller compared to those observed in silica glass at similar pressures (Figure 6) (Coasne et al. 2014). These differences may be due to the synthesis of our glasses under volatile-rich conditions. According to our velocity results using Ne and 4:1 methanol:ethanol, respectively, we observed little change in velocities below ~2.5 GPa. Above ~2.5 GPa, velocities from the run with Ne as the pressure medium begin to diverge from the velocities from the run where 4:1 methanol:ethanol was used as the pressure medium. We note that using Ne as the pressure medium may alter the elasticity of glasses at higher pressures in DAC studies, but does not display any noticeable effects on rhyolitic glasses in the pressure range investigated here.

Discussion

At ambient pressure and relatively low pressures (<1 GPa), the incorporation of H_2O species decreases acoustic velocities and elastic moduli because dissolved H_2O is much more compressible than the surrounding silicate network (Figure 4, 8) (Richet and Polian 1998). The effects of hydration on V_S are larger than those on V_P due to depolymerization of the glass network due to OH^- (Stolper 1982a, 1982b; Deschamps et al. 2011). At higher pressures, interactions between the silicate glass network and H_2O species result in the observed non-linear trends in sound velocities and elastic moduli. The anomalous pressure-dependence of sound velocities in silicate glasses has been attributed to their compression mechanism. Rather than reducing bond lengths, glasses are compressed by collapse of interstitial void spaces and changing of bond angles between bridging tetrahedra (Weigel et al. 2012; Clark et al. 2014; Wang et al. 2014). The transition at which acoustic velocities reach their minima as a function of

This is the peer-reviewed, final accepted version for American Mineralogist, published by the Mineralogical Society of America.
The published version is subject to change. Cite as Authors (Year) Title. American Mineralogist, in press.
DOI: https://doi.org/10.2138/am-2021-7597. http://www.minsocam.org/

pressure has been associated with a tetrahedral packing limit, above which the compression mechanism changes in silicate glasses (Wang et al. 2014). The hydrous glasses in this study have different transition pressures compared to that of AHRG in both V_P and V_S; the transition pressure appears to decrease with increasing H_2O_t (Figure 6). The presence of H_2O_m in interstitial sites may contribute to this shift in transition pressure with increasing H_2O_t. The packing limit of hydrous glasses is reached at lower pressures below ~1.5 GPa because H_2O_m in interstitial sites is more compressible than the anhydrous silicate network (Figure 8). That is, higher quantities of H_2O_t allow the glass to be compressed more easily at pressures below ~1.5 GPa. The transition pressure in V_P occurs below ~2 GPa whereas it occurs above ~1.5-2 GPa in V_S in all glasses, indicating that G is less responsive to the packing limit in hydrous glasses. While K_S begins increasing in both hydrous glasses at ~0.75 GPa, G only begins to increase above ~1.5 GPa. Between ~0.75-1.5 GPa, H_2O_m in interstitial sites prevents compression of the surrounding silicate network and causes K_S in hydrous glasses to converge with K_S in AHRG. Indiscernible K_S between hydrous and anhydrous glasses above ~1.5 GPa indicate that the silicate glass network controls compression at these pressures.

The incorporation of volatiles in interstitial sites has also been shown to flatten the pressure dependence of acoustic velocities (Weigel et al. 2012; Coasne et al. 2014; Clark et al. 2016). Similarly, V_P of hydrous glasses in this study show flatter slopes as a function of pressure below their transition pressures. In contrast, the V_P-pressure slopes are higher in hydrous glasses above their transition pressures. As a result of the lower transition pressure and the steeper V_P-pressure slope above its transition pressure, V_P in HRG-6, which contains abundant H_2O_m, exceeds V_P in both HRG-3 and AHRG above ~1.5 GPa (Figure 6). The more positive slopes and crossover in V_P can be attributed to the presence of H_2O_m in interstitial voids, which causes

372 incompressibility in hydrous glasses to converge with those in AHRG (Figure 8). Because
373 hydrous glasses are intrinsically less dense than AHRG, their bulk moduli eventually become
374 very similar above their transition pressures. While V_S-pressure slopes among all glasses are
375 relatively similar below ~1.5 GPa, V_S in both hydrous glasses converge with AHRG above ~1.5
376 GPa. Based on modeled velocities, it appears that V_S in hydrous glasses will crossover and
377 become higher than those in AHRG above 3 GPa. These results imply that the effects of
378 hydration on acoustic velocities and elastic moduli are non-linear at high pressures up to 3 GPa.

379 **Implications**

380 The non-linear effects of H_2O on acoustic velocities and elastic moduli reported here
381 imply that different water species may also alter acoustic velocities and elastic moduli differently
382 at different P-T conditions relevant to felsic magma chambers at depth. These results could thus
383 be used to provide some insight into the behavior of hydrous felsic silicate melts at depth, given
384 that experimental results at such conditions are still not feasible. For example, the non-linear
385 hydration effects reported here result in lower V_P and K_S at ambient pressure and 300 K
386 compared to the linear hydration effects observed in previous studies (Figure 9) (Meister et al.
387 1980; Suito et al. 1992; Malfait et al. 2011; Whittington et al. 2012). Using these previously
388 determined linear hydration effects to estimate H_2O_t from seismic measurements would thus
389 result in overestimation of H_2O_t in rhyolitic melts. At high temperatures, however, there are a
390 number of factors that may affect the non-linear hydration effects reported here. For instance, the
391 effects of temperature on water speciation can be significant at magmatic temperatures (~650-
392 800 °C): the ratio of OH^- to H_2O_m will increase dramatically compared to that at ambient
393 temperature (Keppler and Bagdassarov 1993; Nowak and Behrens 1995; Evans et al. 2016). In
394 contrast, the effects of pressure on altering water speciation at high temperatures up to ~2 GPa

This is the peer-reviewed, final accepted version for American Mineralogist, published by the Mineralogical Society of America.
The published version is subject to change. Cite as Authors (Year) Title. American Mineralogist, in press.
DOI: https://doi.org/10.2138/am-2021-7597. http://www.minsocam.org/

appear to be negligible (Shen and Keppler 1995; Sowerby and Keppler 1999; Behrens and Yamashita 2008; Chertkova and Yamashita 2015). Because OH^- affects acoustic velocities and elastic moduli more than H_2O_m, such an increase in the ratio of OH^- to H_2O_m at high temperatures may increase velocity reductions in hydrous melts at high P-T and could accentuate the non-linear effects of H_2O_t found in this study. Furthermore, silicate liquids are expected to be more compressible than their glass counterparts (Xu et al. 2018). The role of H_2O_m in interstitial voids may thus be enhanced in melts. Such effects could also add to the non-linear hydration effects at high pressures observed here, but should not be too significant at pressures relevant to rhyolitic magma chambers (~0.5 GPa) (Huang et al. 2015; Flinders et al. 2018; Schmandt et al. 2019). In addition to the effects of water on acoustic velocities at high P-T, the direct effects of temperature on acoustic velocities in glasses and melts with varying H_2O_t need to be determined at high P-T conditions in future studies. Taking all these factors into consideration, it is conceivable that the non-linear effects of hydration on acoustic velocities and elastic moduli of silicate melts exists in felsic magma chambers at deep crustal conditions. This, in turn, can significantly affect our understanding of seismic signatures and the dynamic behavior of felsic magmas. Despite their geologic significance, the effects of hydration on sound velocities and elastic moduli have yet to be explored at high temperatures, even at ambient pressure. It is thus essential for future studies to examine the combined effects of pressure, temperature, and H_2O on acoustic velocities and elastic moduli in felsic silicate melts at deep crustal conditions.

Acknowledgements

J.-F. Lin and J.T. Gu acknowledge support from the National Science Foundation (NSF) Geophysics Program (EAR-1916941), NSF Research Experience for Undergraduate Students (REU), and the International Joint Usage Program at the Institute for Planetary Materials. J.E.

Gardner acknowledges support from NSF grant EAR-1725186 and T. Okuchi acknowledges support from JSPS KAKENHI (17H01172).

References

Amin, S.A., Rissi, E.N., McKiernan, K., and Yarger, J.L. (2012) Determining the equation of state of amorphous solids at high pressure using optical microscopy. Review of Scientific Instruments, 83, 033702.

Ardia, P., Di Muro, A., Giordano, D., Massare, D., Sanchez-Valle, C., and Schmidt, M.W. (2014) Densification mechanisms of haplogranite glasses as a function of water content and pressure based on density and Raman data. Geochimica et Cosmochimica Acta, 138, 158–180.

Bailey, R.A., Dalrymple, G.B., and Lanphere, M.A. (1976) Volcanism, structure, and geochronology of Long Valley Caldera, Mono County, California. Journal of Geophysical Research, 81, 725–744.

Behrens, H., and Yamashita, S. (2008) Water speciation in hydrous sodium tetrasilicate and hexasilicate melts: Constraint from high temperature NIR spectroscopy. Chemical Geology, 256, 306–315.

Behrens, H., and Zhang, Y. (2001) Ar diffusion in hydrous silicic melts: Implications for volatile diffusion mechanisms and fractionation. Earth and Planetary Science Letters, 192, 363–376.

Birch, F. (1978) Finite strain isotherm and velocities for single-crystal and polycrystalline NaCl at high pressures and 300°K. Journal of Geophysical Research, 83, 1257.

Borg, L.E., and Clynne, M.A. (1998) The Petrogenesis of Felsic Calc-alkaline Magmas from the Southernmost Cascades, California: Origin by Partial Melting of Basaltic Lower Crust. Journal of Petrology, 39, 1197–1222.

Brandmeier, M., and Wörner, G. (2016) Compositional variations of ignimbrite magmas in the Central Andes over the past 26 Ma — A multivariate statistical perspective. Lithos, 262, 713–728.

Carn, S.A., Pallister, J.S., Lara, L., Ewert, J.W., Watt, S., Prata, A.J., Thomas, R.J., and Villarosa, G. (2009) The Unexpected Awakening of Chaitén Volcano, Chile. Eos, Transactions American Geophysical Union, 90, 205–206.

Chertkova, N., and Yamashita, S. (2015) In situ spectroscopic study of water speciation in the depolymerized Na 2 Si 2 O 5 melt. Chemical Geology, 409, 149–156.

Clark, A.N., Lesher, C.E., Jacobsen, S.D., and Sen, S. (2014) Mechanisms of anomalous compressibility of vitreous silica. Physical Review B - Condensed Matter and Materials Physics, 90, 1–6.

Clark, A.N., Lesher, C.E., Jacobsen, S.D., and Wang, Y. (2016) Anomalous density and elastic properties of basalt at high pressure: Reevaluating of the effect of melt fraction on seismic velocity in the Earth's crust and upper mantle. Journal of Geophysical Research: Solid Earth, 121, 4232–4248.

Coasne, B., Weigel, C., Polian, A., Kint, M., Rouquette, J., Haines, J., Foret, M., Vacher, R., and Rufflé, B. (2014) Poroelastic theory applied to the adsorption-induced deformation of vitreous silica. Journal of Physical Chemistry B, 118, 14519–14525.

Crosweller, H.S., Arora, B., Brown, S.K., Cottrell, E., Deligne, N.I., Guerrero, N.O., Hobbs, L., Kiyosugi, K., Loughlin, S.C., Lowndes, J., and others (2012) Global database on large magnitude explosive volcanic eruptions (LaMEVE). Journal of Applied Volcanology, 1, 4.

Deschamps, T., Martinet, C., Bruneel, J.L., and Champagnon, B. (2011) Soda-lime silicate glass under hydrostatic pressure and indentation: A micro-Raman study. Journal of Physics Condensed Matter.

Dewaele, A., Torrent, M., Loubeyre, P., and Mezouar, M. (2008) Compression curves of transition metals in the Mbar range: Experiments and projector augmented-wave calculations. Physical Review B, 78, 104102.

Evans, B.W., Hildreth, W., Bachmann, O., and Scaillet, B. (2016) In defense of magnetite-ilmenite thermometry in the Bishop Tuff and its implication for gradients in silicic magma reservoirs. American Mineralogist, 101, 469–482.

Flinders, A.F., and Shen, Y. (2017) Seismic evidence for a possible deep crustal hot zone beneath Southwest Washington. Scientific Reports, 7, 1–10.

Flinders, A.F., Shelly, D.R., Dawson, P.B., Hill, D.P., Tripoli, B., and Shen, Y. (2018) Seismic evidence for significant melt beneath the Long Valley. Geology, 46, 799–802.

Fu, S., Yang, J., and Lin, J.-F. (2017) Abnormal Elasticity of Single-Crystal Magnesiosiderite across the Spin Transition in Earth's Lower Mantle. Physical Review Letters, 118, 036402.

Gardner, J.E., and Ketcham, R.A. (2011) Bubble nucleation in rhyolite and dacite melts: temperature dependence of surface tension. Contributions to Mineralogy and Petrology, 162, 929–943.

Grove, T.L., Till, C.B., and Krawczynski, M.J. (2012) The Role of H_2O in Subduction Zone Magmatism. Annual Review of Earth and Planetary Sciences, 40, 413–439.

Guo, X., Chen, Q., and Ni, H.W. (2016) Electrical conductivity of hydrous silicate melts and aqueous fluids: Measurement and applications. Science China Earth Sciences, 59, 889–900.

Helwig, W., Soignard, E., and Tyburczy, J.A. (2016) Effect of water on the high-pressure structural behavior of anorthite-diopside eutectic glass. Journal of Non-Crystalline Solids, 452, 312–319.

Hess, K.U., and Dingwell, D.B. (1996) Viscosities of hydrous leucogranitic melts: a non-Arrhenian model. American Mineralogist, 81, 1297–1300.

Huang, H.-H., Lin, F.-C., Schmandt, B., Farrell, J., Smith, R.B., and Tsai, V.C. (2015) The Yellowstone magmatic system from the mantle plume to the upper crust. Science, 348, 773–776.

Hui, H., and Zhang, Y. (2007) Toward a general viscosity equation for natural anhydrous and hydrous silicate melts. Geochimica et Cosmochimica Acta, 71, 403–416.

Hui, H., Zhang, Y., Xu, Z., and Behrens, H. (2008) Pressure dependence of the speciation of dissolved water in rhyolitic melts. Geochimica et Cosmochimica Acta, 72, 3229–3240.

Ihinger, P.D., Zhang, Y., and Stolper, E.M. (1999) The speciation of dissolved water in rhyolitic melt. Geochimica et Cosmochimica Acta, 63, 3567–3578.

Keppler, H., and Bagdassarov, N.S. (1993) High-temperature FTIR spectra of H 2 O in rhyolite melt to 1300°C. American Mineralogist, 78, 1324–1327.

Kimura, J.-I., Nagahashi, Y., Satoguchi, Y., and Chang, Q. (2015) Origins of felsic magmas in Japanese subduction zone: Geochemical characterizations of tephra from caldera-forming eruptions <5 Ma. Geochemistry, Geophysics, Geosystems, 16, 2147–2174.

Kushiro, I., Yoder, H.S., and Nishikawa, M. (1968) Effect of Water on the Melting of Enstatite. Geological Society of America Bulletin, 79, 1685–1692.

Lee, S.K., and Stebbins, J.F. (2009) Effects of the degree of polymerization on the structure of sodium silicate and aluminosilicate glasses and melts: An 17O NMR study. Geochimica et Cosmochimica Acta, 73, 1109–1119.

Lee, S.K., Cody, G.D., Fei, Y., and Mysen, B.O. (2004) Nature of polymerization and properties of silicate melts and glasses at high pressure. Geochimica et Cosmochimica Acta, 68, 4189–4200.

Lee, S.K., Lin, J.-F., Cai, Y.Q., Hiraoka, N., Eng, P.J., Okuchi, T., Mao, H. -k., Meng, Y., Hu, M.Y., Chow, P., and others (2008) X-ray Raman scattering study of MgSiO3 glass at high pressure: Implication for triclustered MgSiO3 melt in Earth's mantle. Proceedings of the National Academy of Sciences, 105, 7925–7929.

Lee, S.K., Yi, Y.S., Cody, G.D., Mibe, K., Fei, Y., and Mysen, B.O. (2011) Effect of network polymerization on the pressure-induced structural changes in sodium aluminosilicate glasses and melts: 27Al and 17O solid-state NMR study. Journal of Physical Chemistry C, 116, 2183–2191.

Lin, C.C., and Liu, L.G. (2006) Composition dependence of elasticity in aluminosilicate glasses. Physics and Chemistry of Minerals, 33, 332–346.

Liu, J., and Lin, J.-F. (2014) Abnormal acoustic wave velocities in basaltic and (Fe,Al)-bearing silicate glasses at high pressures. Geophysical Research Letters, 41, 8832–8839.

Lowenstern, J.B. (1994) Dissolved volatile concentrations in an ore-forming magma. Geology.

Lu, C., Mao, Z., Lin, J.-F., Zhuravlev, K.K., Tkachev, S.N., and Prakapenka, V.B. (2013) Elasticity of single-crystal iron-bearing pyrope up to 20GPa and 750K. Earth and Planetary Science Letters, 361, 134–142.

Malfait, W.J., Sanchez-Valle, C., Ardia, P., Médard, E., and Lerch, P. (2011) Compositional dependent compressibility of dissolved water in silicate glasses. American Mineralogist, 96, 1402–1409.

517 Malfait, W.J., Verel, R., Ardia, P., and Sanchez-Valle, C. (2012) Aluminum coordination in rhyolite and
518 andesite glasses and melts: Effect of temperature, pressure, composition and water content.
519 Geochimica et Cosmochimica Acta, 77, 11–26.
520 Malfait, W.J., Seifert, R., and Sanchez-Valle, C. (2014) Densified glasses as structural proxies for high-
521 pressure melts: Configurational compressibility of silicate melts retained in quenched and
522 decompressed glasses. American Mineralogist, 99, 2142–2145.
523 McIntosh, I.M., Nichols, A.R.L., Tani, K., and Llewellin, E.W. (2017) Accounting for the species
524 dependance of the 3500 cm-1 H2Ot infrared molar. American Mineralogist, 102, 1677–1689.
525 Meister, R., Robertson, E.C., Werre, R.W., and Raspet, R. (1980) Elastic Moduli of Rock Glasses Under
526 Pressure to 8 Kilobars and Geophysical Implications. Journal of Geophysical Research, 85, 6461–
527 6470.
528 Moore, G., Vennemann, T., and Carmichael, I.S.E. (1995) Solubility of water in magmas to 2 kbar.
529 Geology, 23, 1099.
530 Mysen, B.O., and Richet, P. (2005) Silicate Glasses and Melts: Properties and Structure. Elsevier Science.
531 Newman, S., Stolper, E.M., and Epstein, S. (1986) Measurement of water in rhyolitic glasses : Calibration
532 of an infrared spectroscopic technique vacuum extraction technique . The grain size of the crushed
533 samples can significantly affect. American Mineralogist, 71, 1527–1541.
534 Ni, H., Keppler, H., Manthilake, M.A.G.M., and Katsura, T. (2011) Electrical conductivity of dry and
535 hydrous NaAlSi3O8glasses and liquids at high pressures. Contributions to Mineralogy and
536 Petrology, 162, 501–513.
537 Nowak, M., and Behrens, H. (1995) The speciation of water in haplogranitic glasses and melts determined
538 by in situ near-infrared spectroscopy. Geochimica et Cosmochimica Acta, 59, 3445–3450.
539 Ochs, F.A., and Lange, R.A. (1999) The Density of Hydrous Magmatic Liquids. Science, 283, 1314–
540 1317.
541 Richet, P., and Polian, A. (1998) Water as a dense icelike component in silicate glasses. Science, 281,
542 396–398.
543 Richet, P., Lejeune, A.-M., Holtz, F., and Roux, J. (1996) Water and the viscosity of andesite melts.
544 Chemical Geology, 128, 185–197.
545 Richet, P., Whittington, A., Holtz, F., Behrens, H., Ohlhorst, S., and Wilke, M. (2000) Water and the
546 density of silicate glasses. Contributions to Mineralogy and Petrology, 138, 337–347.
547 Sakamaki, T., Kono, Y., Wang, Y., Park, C., Yu, T., Jing, Z., and Shen, G. (2014) Contrasting sound
548 velocity and intermediate-range structural order between polymerized and depolymerized silicate
549 glasses under pressure. Earth and Planetary Science Letters, 391, 288–295.
550 Sanchez-Valle, C., and Bass, J.D. (2010) Elasticity and pressure-induced structural changes in vitreous
551 MgSiO3-enstatite to lower mantle pressures. Earth and Planetary Science Letters, 295, 523–530.
552 Schmandt, B., Jiang, C., and Farrell, J. (2019) Seismic perspectives from the western U.S. on magma
553 reservoirs underlying large silicic calderas. Journal of Volcanology and Geothermal Research, 384,
554 158–178.
555 Seifert, F.A., Mysen, B.O., and Virgo, D. (1981) Structural similarity of glasses and melts relevant to
556 petrological processes. Geochimica et Cosmochimica Acta, 45, 1879–1884.
557 Shaw, H.R. (1963) Obsidian-H 2 O viscosities at 1000 and 2000 bars in the temperature range 700° to
558 900°C. Journal of Geophysical Research, 68, 6337–6343.
559 Shaw, H.R. (1972) Viscosities of magmatic silicate liquids; an empirical method of prediction. American
560 Journal of Science, 272, 870–893.
561 Shen, A., and Keppler, H. (1995) Infrared spectroscopy of hydrous silicate melts to 1000°C and 10 kbar:
562 direct observation of H2O speciation in a diamond-anvil cell. American Mineralogist, 80, 1335–
563 1338.
564 Shen, G., Mei, Q., Prakapenka, V.B., Lazor, P., Sinogeikin, S., Meng, Y., and Park, C. (2011) Effect of
565 helium on structure and compression behavior of SiO2 glass. Proceedings of the National Academy
566 of Sciences, 108, 6004–6007.
567 Sowerby, J.R., and Keppler, H. (1999) Water speciation in rhyolitic melt determined by in-situ infrared

568 spectroscopy. American Mineralogist, 84, 1843–1849.
569 Stolper, E. (1982a) The speciation of water in silicate melts. Geochimica et Cosmochimica Acta, 46,
570 2609–2620.
571 ——— (1982b) Water in Silicate Glasses: An Infrared Spectroscopic Study. Contributions to Mineralogy
572 and Petrology Mineral Petrol, 81, 1–17.
573 Suito, K., Miyoshi, M., Sasakura, T., and Fujisaw, H. (1992) Elastic Properties of Obsidian, Vitreous
574 SiO2, and Vitreous GeO2 Under High Pressure up to 6 GPa. In High-Pressure Research:
575 Application to Earth and Planetary Sciences Vol. 67, pp. 219–225.
576 Wallace, P.J. (2005) Volatiles in subduction zone magmas: concentrations and fluxes based on melt
577 inclusion and volcanic gas data. Journal of Volcanology and Geothermal Research, 140, 217–240.
578 Wallace, P.J., Anderson, A.T., and Davis, A.M. (1999) Gradients in H 2 O, CO 2 , and exsolved gas in a
579 large-volume silicic magma system: Interpreting the record preserved in melt inclusions from the
580 Bishop Tuff. Journal of Geophysical Research: Solid Earth, 104, 20097–20122.
581 Wang, Y., Sakamaki, T., Skinner, L.B., Jing, Z., Yu, T., Kono, Y., Park, C., Shen, G., Rivers, M.L., and
582 Sutton, S.R. (2014) Atomistic insight into viscosity and density of silicate melts under pressure.
583 Nature Communications, 5, 3241.
584 Weigel, C., Polian, A., Kint, M., Rufflé, B., Foret, M., and Vacher, R. (2012) Vitreous silica distends in
585 helium gas: Acoustic versus static compressibilities. Physical Review Letters, 109, 1–5.
586 Whittington, A., Richet, P., and Holtz, F. (2000) Water and the viscosity of depolymerized
587 aluminosilicate melts. Geochimica et Cosmochimica Acta, 64, 3725–3736.
588 Whittington, A.C., Richet, P., and Polian, A. (2012) Water and the compressibility of silicate glasses: A
589 Brillouin spectroscopic study. American Mineralogist, 97, 455–467.
590 Williams, Q., and Jeanloz, R. (1998) Spectroscopic Evidence for Pressure-Induced Coordination Changes
591 in Silicate Glasses and Melts. Science, 239, 902–905.
592 Withers, A.C., and Behrens, H. (1999) Temperature-induced changes in the NIR spectra of hydrous
593 albitic and rhyolitic glasses between 300 and 100 K. Physics and Chemistry of Minerals, 27, 119–
594 132.
595 Withers, A.C., Zhang, Y., and Behrens, H. (1999) Reconciliation of experimental results on H2O
596 speciation in rhyolitic glass using in-situ and quenching techniques. Earth and Planetary Science
597 Letters, 173, 343–349.
598 Xu, M., Jing, Z., Chantel, J., Jiang, P., Yu, T., and Wang, Y. (2018) Ultrasonic Velocity of Diopside
599 Liquid at High Pressure and Temperature: Constraints on Velocity Reduction in the Upper Mantle
600 Due to Partial Melts. Journal of Geophysical Research: Solid Earth, 123, 8676–8690.
601 Yang, J., Mao, Z., Lin, J.F., and Prakapenka, V.B. (2014) Single-crystal elasticity of the deep-mantle
602 magnesite at high pressure and temperature. Earth and Planetary Science Letters, 392, 292–299.
603 Yokoyama, A., Matsui, M., Higo, Y., Kono, Y., Irifune, T., and Funakoshi, K. (2010) Elastic wave
604 velocities of silica glass at high temperatures and high pressures. Journal of Applied Physics, 107,
605 123530.
606 Zha, C.-S., Hemley, R.J., Mao, H., Duffy, T.S., and Meade, C. (1994) Acoustic velocities and refractive
607 index of SiO2 glass to 57.5 GPa by Brillouin scattering. Physical Review B, 50, 13105–13112.
608 Zhang, Y., Belcher, R., Ihinger, P.D., Wang, L., Xu, Z., and Newman, S. (1997) New calibration of
609 infrared measurement of dissolved water in rhyolitic glasses. Geochimica et Cosmochimica Acta,
610 61, 3089–3100.
611
612
613
614
615
616
617

Figure Captions

Figure 1. Representative raw FTIR spectra of rhyolitic glasses at ambient conditions. Numbers in parentheses represent sample thicknesses. The absorption bands are assigned and labeled with the associated H_2O species based on previous studies (Stolper 1982b; Newman et al. 1986; Withers and Behrens 1999). MIR spectra (< 4000 cm^{-1}) were only recorded for thin samples (< ~30 μm) whereas NIR spectra (> 4000 cm^{-1}) allow for comparison between thicker samples. The modulations in the MIR spectrum of AHRG are fringes resulting from the double-side polished sample.

Figure 2. Representative Brillouin Light Scattering spectra of rhyolitic glasses at ~3 GPa. (**a**) anhydrous (AHRG) and (**b** and **c**) hydrous with 3.28 wt% H_2O_t (HRG-3) and 5.90 wt% H_2O_t (HRG-6). Open circles are experimental data and red lines show fitted Gaussian peaks. The compressional (V_P) and shear (V_S) wave velocities of the glasses and Ne are labeled. The insert in (**b**) shows the sample chamber in a DAC that has been loaded with AHRG (lower left), HRG-6 (upper right), ruby as the pressure calibrant (upper left), and Ne as the pressure medium.

Figure 3. Representative FTIR spectra of the two hydrous rhyolitic glasses with increasing pressure. (**a**) FTIR spectra of HRG-6 (5.90 wt% H_2O_t) in the mid-IR region. (**b**) FTIR spectra of HRG-3 (3.28 wt% H_2O_t) in the near-IR region. Linear baselines were subtracted from the mid-IR spectra in (a) whereas flexicurve baselines were used for background subtraction from the near-IR spectra in (**b**) (Newman et al. 1986; Withers and Behrens 1999; McIntosh et al. 2017). Ne was used as the pressure medium in FTIR experiments.

Figure 4. Comparison of acoustic velocities in rhyolitic and haplogranitic glasses as a function of total water content (H_2O_t) at ambient conditions. Red symbols represent acoustic velocities in rhyolitic glasses whereas open black symbols represent acoustic velocities in haplogranitic glasses. The dashed red lines are linear fits to the data for rhyolitic glasses while the dashed black lines are linear best-fit lines for haplogranitic glasses similar to those used by Malfait et al. (2011). Uncertainties are smaller than symbols when not shown.

Figure 5. Calculated H_2O speciation in the two hydrous rhyolitic glasses (HRG-3 and HRG-6). Abundance of hydroxyl groups (OH^-) is depicted by circles while abundance of molecular water (H_2O_m) is depicted by squares. Error bars are shown for HRG-6 (5.90 wt% H_2O_t) whereas they lie within the symbols for HRG-3 (3.28 wt% H_2O_t). Literature data from (Hui et al. 2008) are shown as open symbols where red symbols indicate glasses with < 2 wt% H_2O_t and orange symbols represent glasses with 2-4.16 wt% H_2O_t.

Figure 6. Acoustic velocities in anhydrous and hydrous rhyolitic glasses as a function of pressure. (**a**) Compressional wave velocities (V_P), (**b**) shear wave velocities (V_S), and (**c**) percent differences in velocity ($100*(V_{hydrous} - V_{anhydrous})/V_{anhydrous}$) between hydrous glasses and the anhydrous glass in this study. In (**a**) and (**b**), solid circles are experimental data from BLS-Run 1 and BLS-Run 3 where Ne was used as the pressure medium. Solid squares are experimental data from BLS-Run 2 where 4:1 methanol:ethanol (ME) was used as the pressure medium. Solid lines are modeled velocity profiles using data from the BLS-Run 1 and BLS-Run 3. Open symbols are literature data on haplogranitic or rhyolitic glasses: open squares (Malfait et al. 2011), open

circles (Whittington et al. 2012), and open triangles (Meister et al. 1980). Dashed lines are velocity profiles for SiO_2 glasses with either Ne (green, Coasne et al. 2014) or ME (magenta, Weigel et al. 2012) as the pressure medium. In (**c**), solid lines represent percent differences in V_P, dashed lines represent percent differences in V_S, and vertical ticks represent error bars. The color of the lines corresponds to the glass sample they represent (red- AHRG, orange- HRG-3, and blue- HRG-6).

Figure 7. Modeled density-pressure relationships of anhydrous and hydrous rhyolitic glasses. Solid symbols represent densities calculated from our measured sound velocities with Ne as the pressure medium. Solid lines are best fits from equation-of-state modeling (Birch 1978). Open symbols are literature data on haplogranitic or rhyolitic glasses: open squares (Malfait et al. 2011), open circles (Whittington et al. 2012), and open triangles (Ardia et al. 2014). Dashed lines are polynomial fits to the data from Ardia et al. (2014). The insert shows modeled percent differences in density ($100*(\rho_{hydrous} - \rho_{anhydrous})/\rho_{anhydrous}$) between hydrous glasses and the anhydrous glass in this study.

Figure 8. Adiabatic bulk moduli and shear moduli of anhydrous and hydrous rhyolitic glasses as a function of pressure. Solid symbols represent elastic moduli calculated from measured sound velocities with Ne as the pressure medium. Solid lines are best fits from equation-of-state fitting (Birch 1978). Uncertainties are smaller than symbols. Open symbols are literature data on haplogranitic or rhyolitic glasses: open squares Open symbols are literature data on haplogranitic or rhyolitic glasses: open squares (Malfait et al. 2011), open circles (Whittington et al. 2012), open triangles (Meister et al. 1980), and open diamonds (Suito et al. 1992).

Figure 9. Modeled compressional wave velocities, bulk moduli, and density of hydrous glasses at pressures relevant to magmatic processes. (**a**) Compressional wave velocities, (**b**) bulk moduli, and (**c**) densities of rhyolitic glasses as functions of H_2O_t. Solid lines are parabolic fits of the velocity and equation of state parameters at each given pressure. Dashed lines represent linear fits to ambient pressure literature data for rhyolitic glasses from this study, Meister et al. (1980), Suito et al. (1992), Whittington et al. (2012).

Tables

Table 1. Synthesis conditions of rhyolitic glasses. Values in parentheses are standard deviations from FTIR measurements.

Sample	Run	P (MPa)	T (°C)	Time (hrs)	OH^- (wt%)	H_2O_m (wt%)	H_2O_t (wt%)
HRG-6	G-1730	190	850	169	1.67 (10)	4.23 (17)	5.90 (20)
AHRG	G-1756	0.5	1150	41.5	-	-	< 0.15
HRG-3	G-1800	67.5	875	165	1.58 (6)	1.70 (7)	3.28 (9)

Table 2. Compositions and total water contents (H_2O_t) of glasses in this study. The sum of components other than H_2O_t are normalized to 100% for comparison between different glass samples. Values in parentheses are standard deviations from EPMA and FTIR measurements.

Oxide wt%	Whole-Rock	AHRG	HRG-3	HRG-6
SiO_2	76.53	76.70 (98)	76.23 (67)	76.46 (97)
Al_2O_3	13.01	13.30 (18)	13.37 (19)	13.23 (22)
Na_2O	3.87	4.00 (40)	3.67 (3)	3.85 (17)
K_2O	4.91	4.85 (21)	4.99 (7)	4.91 (10)
CaO	0.74	0.82 (5)	0.77 (3)	0.75 (3)
FeO	0.79	0.23 (14)	0.84 (10)	0.67 (9)
MgO	0.02	0.03 (2)	0.02 (1)	0.02 (2)
MnO	0.08	0.02 (2)	0.05 (1)	0.06 (2)
TiO_2	0.06	0.04 (3)	0.05 (3)	0.05 (2)
H_2O_t	-	< 0.15	3.28 (9)	5.90 (18)

780 **Table 3.** Ambient pressure acoustic velocities, elastic moduli, and densities of investigated
781 glasses. Values in parentheses are estimated uncertainties for velocities and densities, whereas
782 they are standard deviations from equation of state fitting for elastic moduli.

	AHRG (BLS-Run 1)	**HRG-3 (BLS-Run 3)**	**HRG-6 (BLS-Run 1)**
V_P **(km/s)**	5.87 (3)	5.59 (3)	5.57 (3)
V_S **(km/s)**	3.63 (3)	3.38 (3)	3.32 (3)
K_S **(GPa)**	39.7 (3)	36.9 (4)	37.2 (4)
K_S' **(no unit)**	-3.7 (3)	-1.4 (6)	-2.2 (4)
K_S'' **(GPa^{-1})**	1.9 (1)	1.7 (3)	2.2 (2)
G **(GPa)**	31.0 (2)	26.6 (2)	25.0 (2)
G' **(no unit)**	-1.7 (2)	-1.4 (3)	-1.5 (2)
G'' **(GPa^{-1})**	0.4 (1)	0.6 (2)	1.1 (1)
Density (g/cm^3)	2.353 (5)	2.270 (5)	2.318 (5)

783

Figure 1

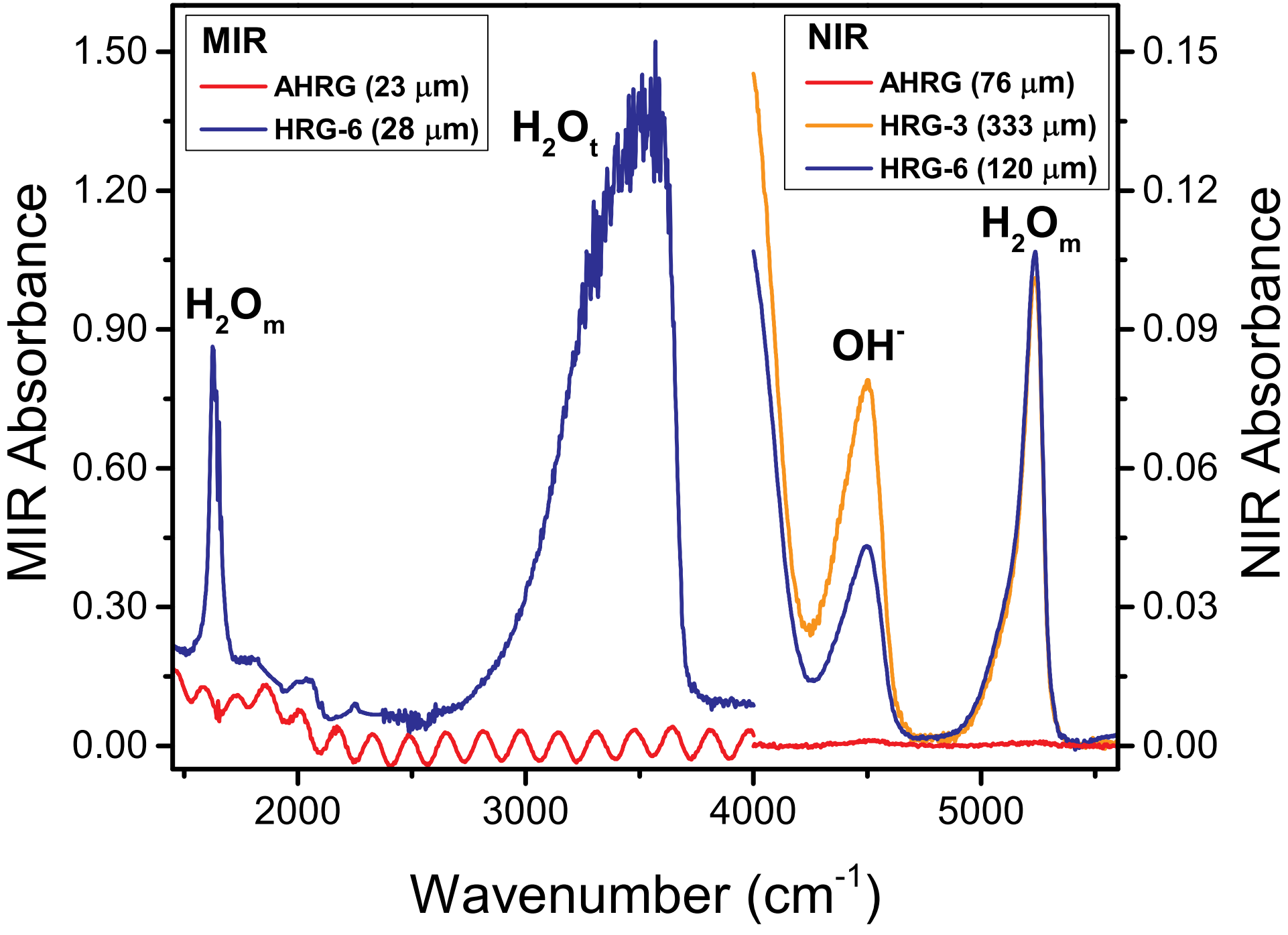
MIR
AHRG (23 μm)
HRG-6 (28 μm)
NIR
AHRG (76 μm)
HRG-3 (333 μm)
HRG-6 (120 μm)
H2Om
H2Ot
OH-
H2Om
MIR Absorbance
NIR Absorbance
Wavenumber (cm-1)
1.50
1.20
0.90
0.60
0.30
0.00
0.15
0.12
0.09
0.06
0.03
0.00
2000
3000
4000
5000

Figure 2

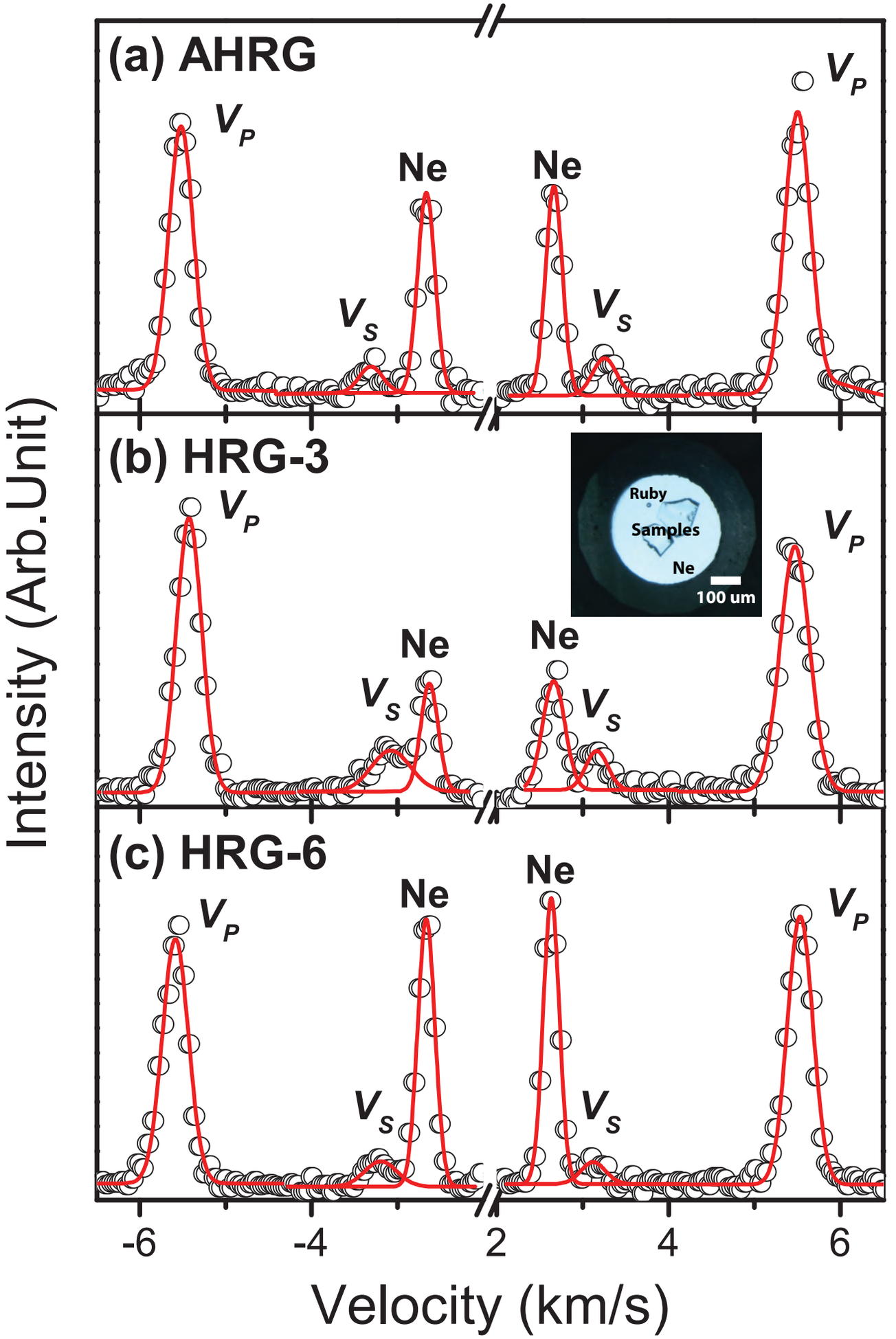
(a) AHRG
(b) HRG-3
(c) HRG-6
V_P
V_S
Ne
Ruby
Samples
Ne
100 um
Intensity (Arb.Unit)
-6
-4
2
4
6
Velocity (km/s)

Figure 3

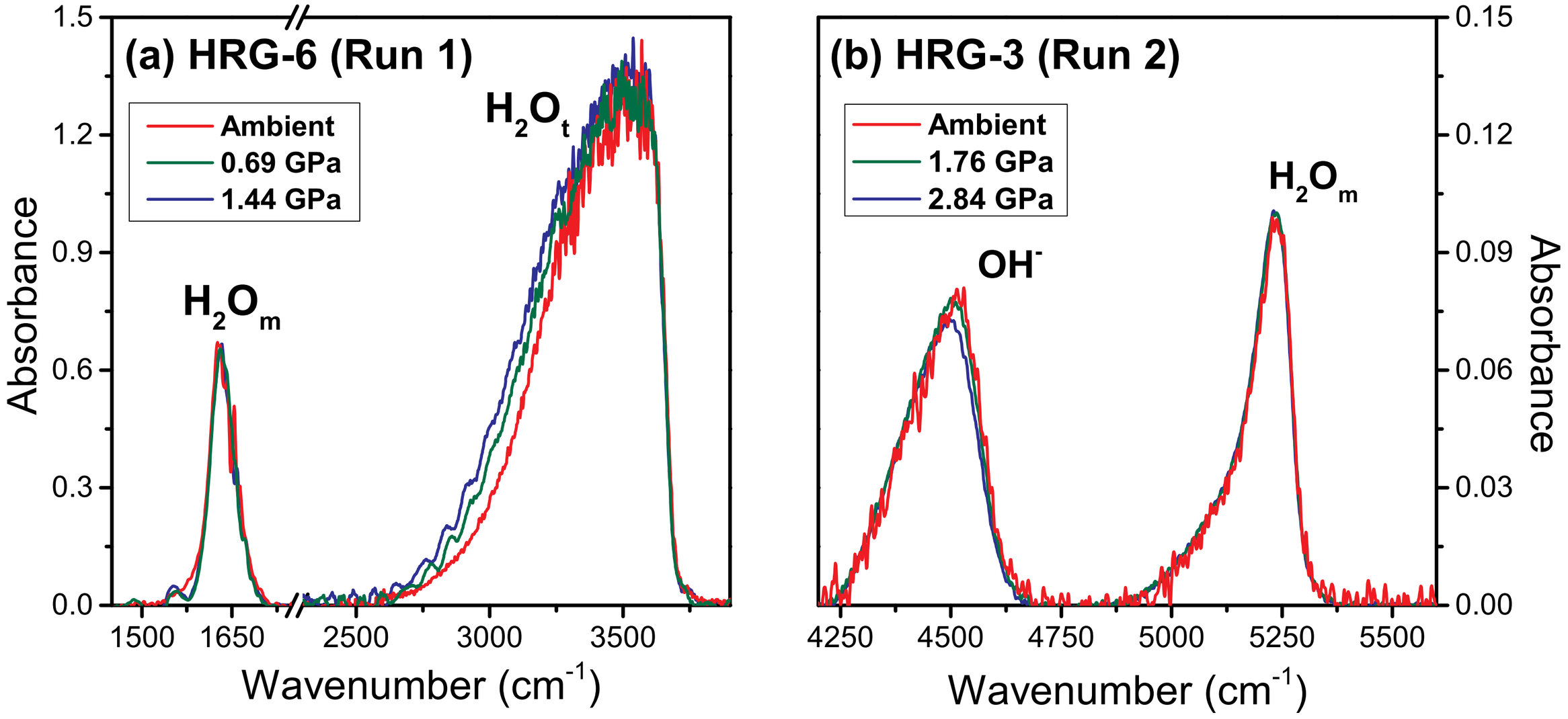
(a) HRG-6 (Run 1)
Ambient
0.69 GPa
1.44 GPa
H_2O_t
H_2O_m
Absorbance
Wavenumber (cm^{-1})
1.5
1.2
0.9
0.6
0.3
0.0
1500
1650
2500
3000
3500
(b) HRG-3 (Run 2)
Ambient
1.76 GPa
2.84 GPa
H_2O_m
OH^-
Absorbance
Wavenumber (cm^{-1})
0.15
0.12
0.09
0.06
0.03
0.00
4250
4500
4750
5000
5250
5500

Figure 4

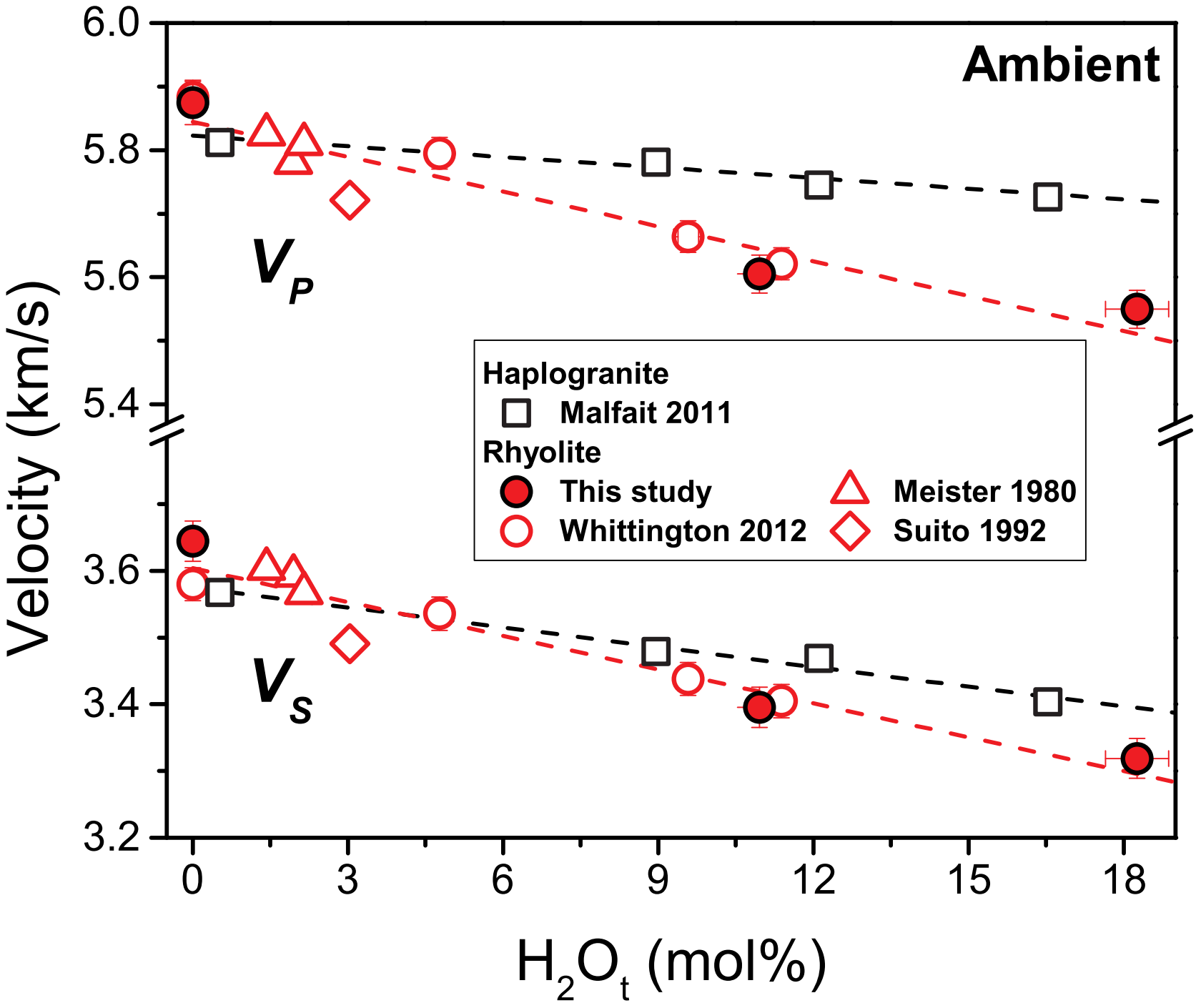
Ambient
V_P
V_S
Velocity (km/s)
6.0
5.8
5.6
5.4
3.6
3.4
3.2
0
3
6
9
12
15
18
H_2O_t (mol%)
Haplogranite
Malfait 2011
Rhyolite
This study
Whittington 2012
Meister 1980
Suito 1992

Figure 5

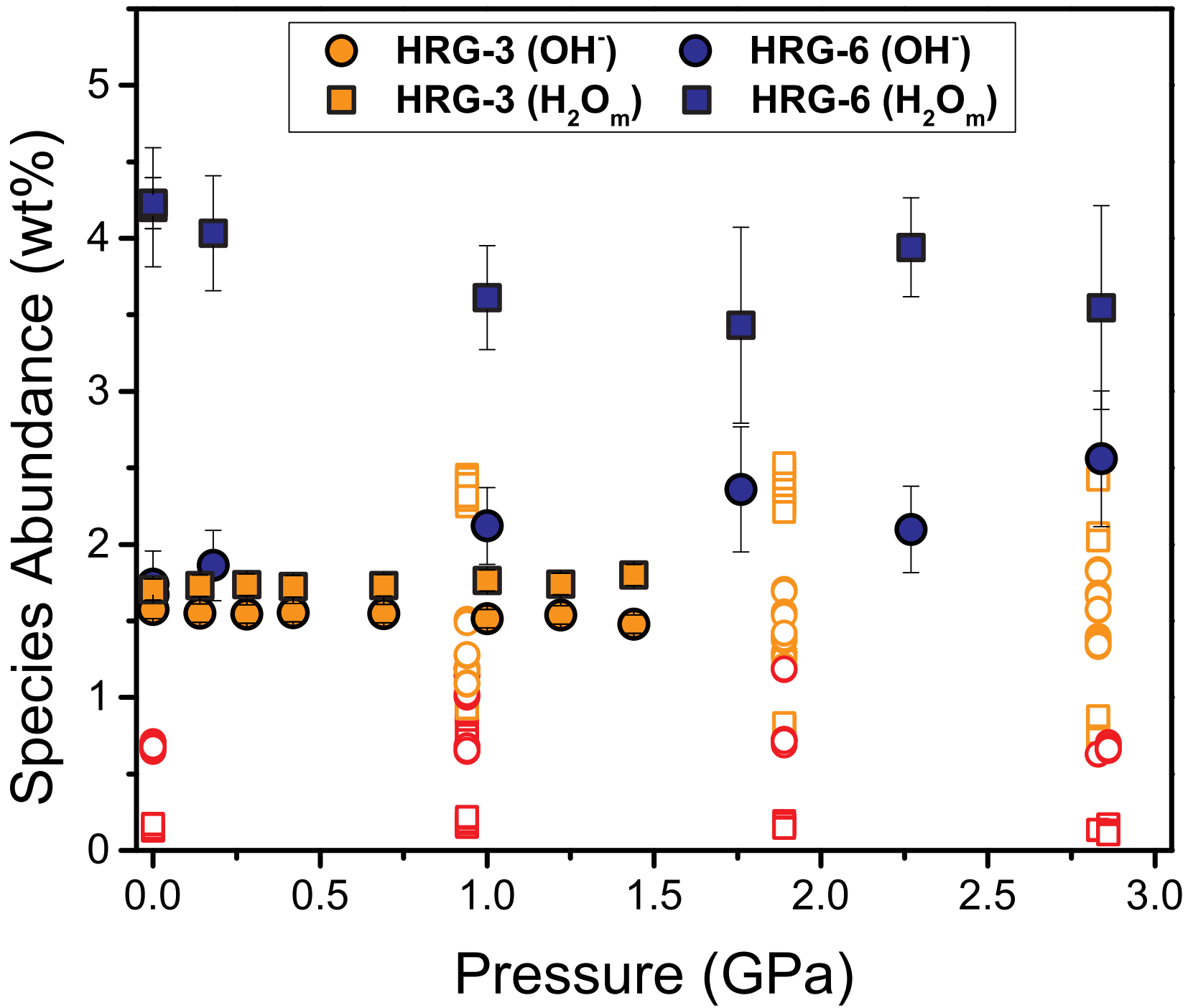
HRG-3 (OH-)
HRG-6 (OH-)
HRG-3 (H2Om)
HRG-6 (H2Om)
Species Abundance (wt%)
Pressure (GPa)
0
1
2
3
4
5
0.0
0.5
1.0
1.5
2.0
2.5
3.0

Figure 6

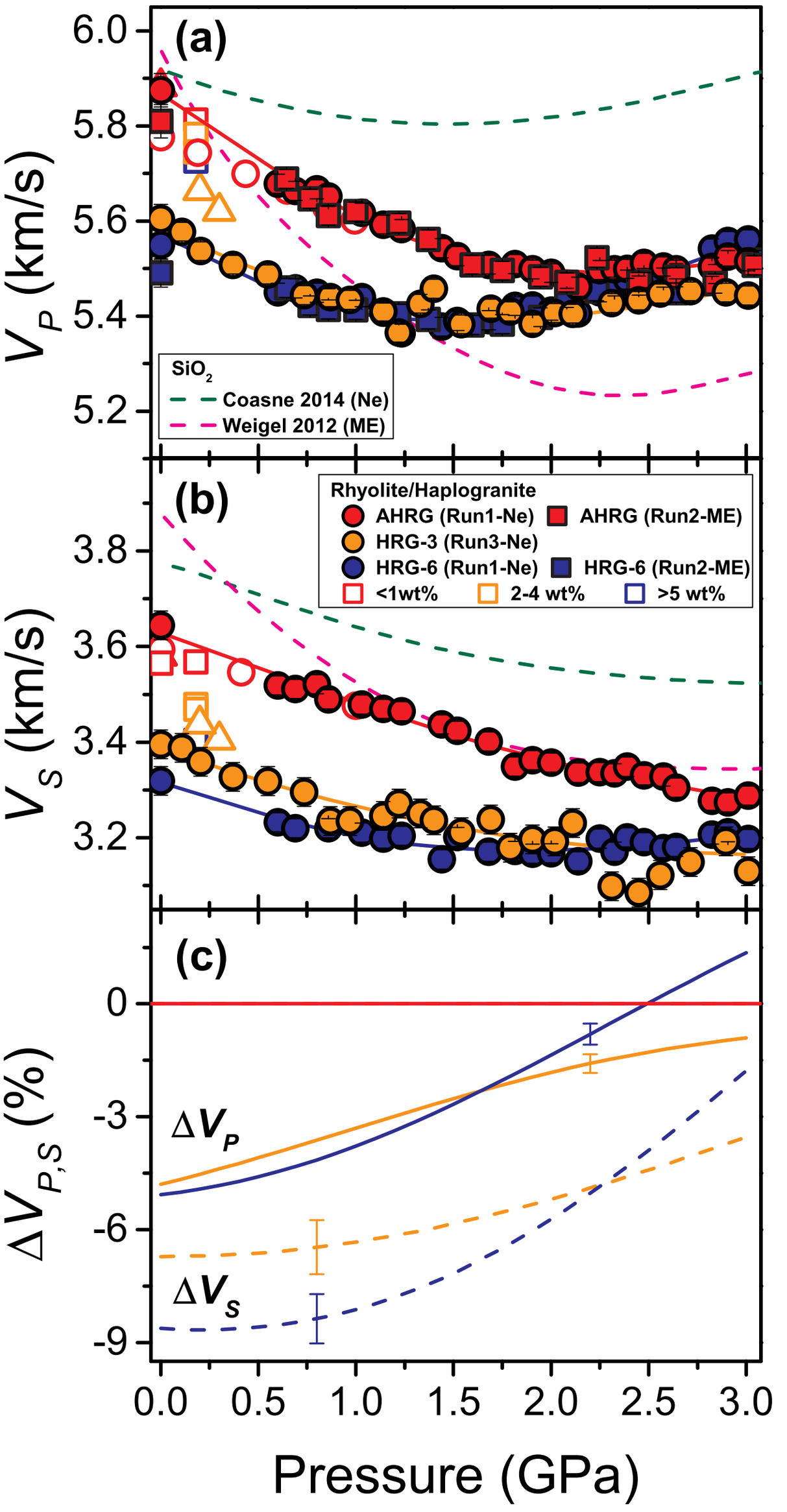
(a)
6.0
5.8
5.6
5.4
5.2
V_P (km/s)
SiO2
Coasne 2014 (Ne)
Weigel 2012 (ME)
(b)
3.8
3.6
3.4
3.2
V_S (km/s)
Rhyolite/Haplogranite
AHRG (Run1-Ne)
AHRG (Run2-ME)
HRG-3 (Run3-Ne)
HRG-6 (Run1-Ne)
HRG-6 (Run2-ME)
<1wt%
2-4 wt%
>5 wt%
(c)
0
-3
-6
-9
$\Delta V_{P,S}$ (%)
ΔV_P
ΔV_S
0.0
0.5
1.0
1.5
2.0
2.5
3.0
Pressure (GPa)

Figure 7

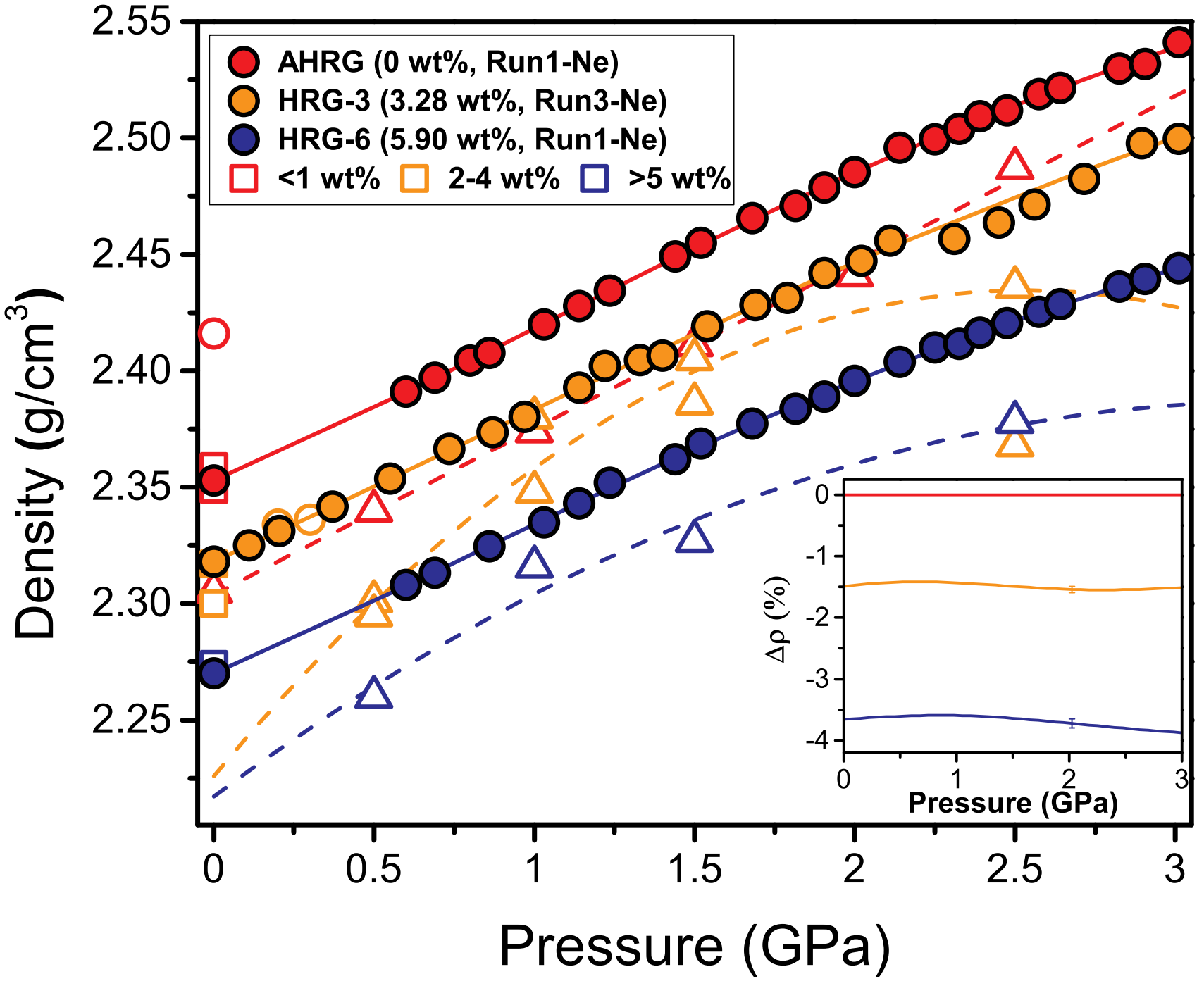
AHRG (0 wt%, Run1-Ne)
HRG-3 (3.28 wt%, Run3-Ne)
HRG-6 (5.90 wt%, Run1-Ne)
<1 wt%
2-4 wt%
>5 wt%
Density (g/cm3)
Pressure (GPa)
Δρ (%)
Pressure (GPa)

Figure 8

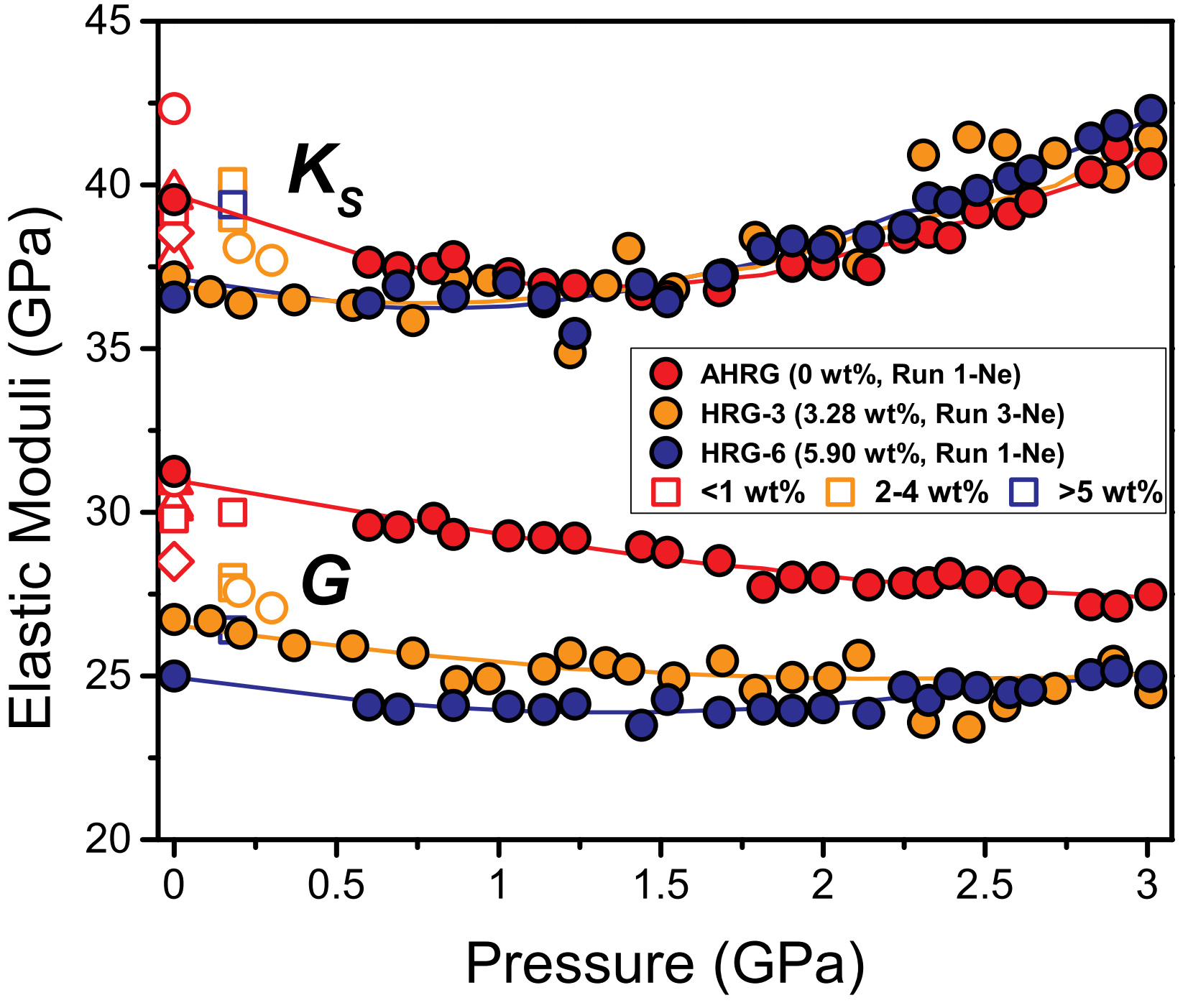
Elastic Moduli (GPa)
Pressure (GPa)
45
40
35
30
25
20
0
0.5
1
1.5
2
2.5
3
K_S
G
AHRG (0 wt%, Run 1-Ne)
HRG-3 (3.28 wt%, Run 3-Ne)
HRG-6 (5.90 wt%, Run 1-Ne)
<1 wt%
2-4 wt%
>5 wt%

Figure 9

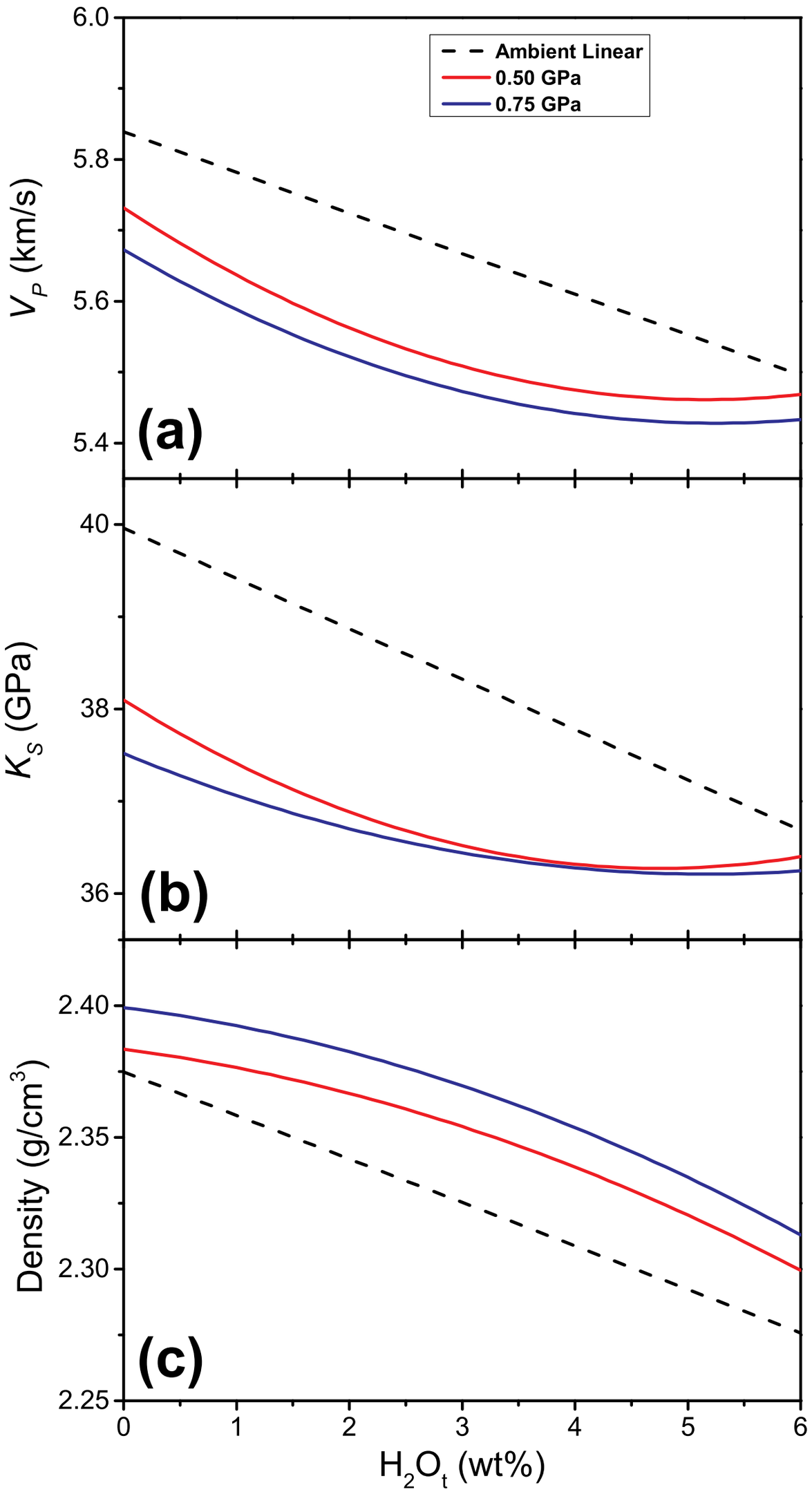
Ambient Linear
0.50 GPa
0.75 GPa
V_P (km/s)
6.0
5.8
5.6
5.4
(a)
K_S (GPa)
40
38
36
(b)
Density (g/cm^3)
2.40
2.35
2.30
2.25
(c)
0
1
2
3
4
5
6
H_2O_t (wt%)